Design and Transient Studies on Multi-Terminal VSC-HVDC Systems Interconnecting Offshore Wind Farms

M. Mohan[*†] and **K. Panduranga Vittal**[**], Non-members

ABSTRACT

In recent years, offshore wind energy has increased significantly. The continuous increase in the offshore wind power generation level brings the requirement of offshore wind farms (OWFs) integration with an AC grid. The multi-terminal (MT) voltage source converters (VSC)-based high voltage direct current (HVDC) transmission system is an emerging technology and also the best option to interconnect the large-scale OWFs to the AC grid. This paper presents the design, modeling, and control of MT VSC-HVDC transmission system linked offshore wind farms. Different cases of MT VSC-HVDC transmission systems are developed, and its simulation studies are carried out using PSCAD/EMTDC. The test results show the transient performance of the MT VSC-HVDC transmission systems under various AC and DC fault conditions. The studies also include the influence of wind variabilities as in the form of gust and ramp pattern during steady state and fault conditions.

Keywords: MT VSC-HVDC system, Offshore wind farms, Power system transients, Voltage source converters, Wind energy integration.

1. INTRODUCTION

Electricity generation from renewable energy sources is continuously increasing due to its environmental and economic advantages. Wind power generation is one of the best options to produce green power without any harmful emissions. Recently, offshore wind farms (OWFs) are the emerging technology of wind energy systems [1]. Due to the problem of uncontrollable variation and random generation, it is very difficult to connect the OWFs with the customers directly; instead, it can be integrated with the grid. The large-scale OWFs can be integrated with the AC grid via high voltage alternating current (HVAC) or high voltage direct current (HVDC) link. The HVDC transmission is the economical option for long-distance bulk power transmission due to low losses and absence of capacitance effect [2]. At first, the HVDC systems are developed based on thyristors, i.e., line-commutated converters (LCC)-based HVDC. Recently, the use of voltage source converters (VSC) into the HVDC systems has increased due to the capability of fault current blocking and operation with weak AC systems like OWFs [3]. In the multi-terminal (MT) HVDC network, the power flow cannot be interrupted even if the fault occurs in a DC line, and it requires a smaller number of terminals. Therefore, the MT VSC-HVDC transmission system is the beneficial option for connecting the OWFs with an AC grid.

The authors of [4] have presented new control strategies to provide the coordination between VSC transmission and DFIG based wind farms under variable wind and power generation conditions as well as grid fault conditions. In [5], the dynamic performance of a 200 MW, ±100kV VSC-HVDC transmission system under fault conditions are presented. Authors of [6] have analyzed the performance of hybrid HVDC systems such as the line-commutated converter-based HVDC in combination with VSC linked OWFs under variable wind and fault situations. In [7], the analysis of steady state, dynamic and transient behavior of the MT VSC-HVDC transmission systems are presented.

In this paper, the design, modeling, and control of the MT VSC-HVDC transmission system linked OWFs are presented. Different cases of MT VSC-HVDC transmission systems are modeled, and its simulation studies are carried out in PSCAD/EMTDC to analyze the transient performance of the MT VSC-based HVDC systems under variable wind and fault conditions.

This paper is organized as follows. Section 2 discusses the design and modeling of MT VSC-HVDC systems. Section 3 presents the simulation analysis of the modeled HVDC systems under fault conditions including wind variabilities. Finally, Section 4 concludes with the important points which are observed in the simulation analysis.

2. MULTI-TERMINAL VSC-HVDC SYSTEM LINKED OFFSHORE WIND FARMS

The configuration of the MT VSC-HVDC transmission system which can be used to connect the OWFs with an AC grid is presented in Fig. 1.

The design of the MT VSC-HVDC system can be

Manuscript received on October 21, 2018 ; revised on July 13, 2019 ; accepted on August 27, 2019.

*The author is with CMR Institute of Technology, Bengaluru, India. E-mail : mohanbe.m@gmail.com

**The author is with National Institute of Technology Karnataka (NITK), Surathkal, Mangalore, India.

†Corresponding author.

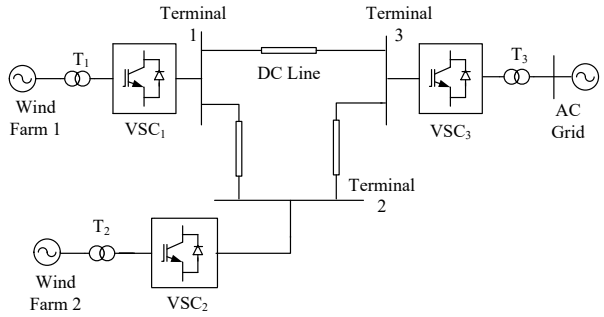

Fig.1: *MT VSC-HVDC transmission system linked OWFs.*

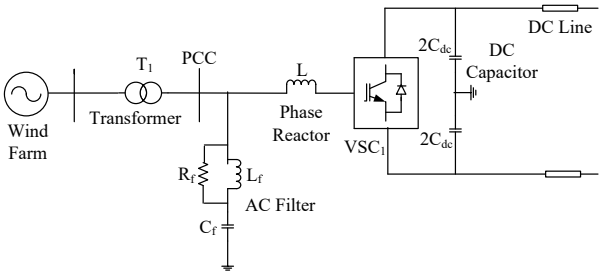

Fig.2: *Wind farm connected HVDC converter. (where, PCC refers to Point of Common Coupling).*

done using the modeling of one HVDC converter station. Fig. 2 shows the schematic diagram of an OWF which has been connected to the HVDC converter. It contains the OWF, converter transformer, AC filter, phase reactor, VSC, DC capacitor and DC transmission line.

2.1 Wind Power Generation System

The wind power generation unit consists of the wind turbine and permanent magnet synchronous generator (PMSG). The wind turbine produces the mechanical power by taking the input as wind speed. The shaft of the PMSG is coupled with the wind turbine through the gearbox. The generated mechanical power is given as input to the PMSG, and it produces the electrical power with the help of permanent magnets. The following relations can describe the modeling of the wind turbine and PMSG.

The mechanical power output of the wind turbine depends on the wind speed, power coefficient, air density and the area of the rotor blade. It is given by,

$$P_m = \frac{1}{2}\rho A v^3 C_p(\theta, \lambda) \tag{1}$$

where ρ is the air density, A is the swept area of the rotor in m^2, v is the wind speed in m/s, C_p is the power coefficient, and it depends on the pitch angle of rotor blades (θ) and the tip speed ratio (λ). It can be determined using the following relations,

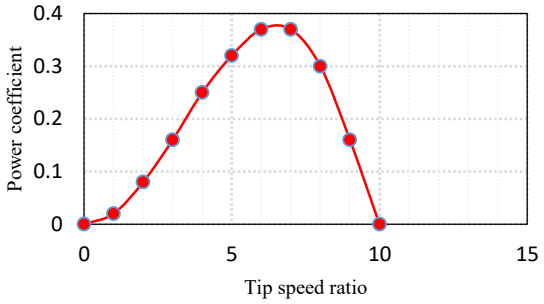

Fig.3: *Power coefficient vs tip speed ratio curve.*

$$C_p = 0.73\left(\frac{151}{\lambda_i} - 0.58\theta - 0.002\theta^{2.14} - 13.2\right)e^{\frac{-18.4}{\lambda_i}} \tag{2}$$

$$\frac{1}{\lambda_i} = \frac{1}{\lambda - 0.02\theta} - \frac{0.003}{\theta^3 + 1} \tag{3}$$

tip speed ratio,

$$\lambda = \frac{\omega_r R}{v} \tag{4}$$

where ω_r is the rotational speed of rotor in rad/sec, and R is the radius of rotor blade in m [8, 9]. Fig. 3 shows the tip speed ratio vs power coefficient curve.

The dynamic model of the wind turbine is given by,

$$J\frac{d\omega_r}{dt} + B\omega_r = T_m - T_e \tag{5}$$

where J and B are the inertia and friction coefficient, T_m is the turbine mechanical torque, and T_e is the electromagnetic torque [10].

The PMSG is highly preferable for the wind energy systems. The dynamic model of the PMSG is developed by using the voltage and flux equations, and it is not developed based on the equations of rotor winding due to its permanent magnets. It can be expressed using the rotor frame.

The stator voltage in $d-q$ axis is given by,

$$V_{qs} = r_s i_{qs} + \omega_r L_d i_{ds} + \omega_r \lambda_m + L_q \frac{di_{qs}}{dt} \tag{6}$$

$$V_{ds} = r_s i_{ds} + L_d \frac{di_{ds}}{dt} - \omega_r L_q i_{qs} \tag{7}$$

where r_s and L_s are the stator winding resistance and inductance, λ_m is the flux linkages created by permanent magnets. L_d and L_q are the inductance of the generator on the d and q axis. i_{ds} and i_{qs} are the stator currents in the $d-q$ axis.

The electromagnetic torque is given by,

$$T_e = \left(\frac{3}{2}\right)\left(\frac{p}{2}\right)\left(\lambda_m i_{qs} + (L_d - L_q) i_{qs} i_{ds}\right) \tag{8}$$

where p is the number of poles [11, 12].

2.2 Converter Transformer

The converter transformer can be applied to change the grid or OWF AC voltage to the suitable rating of VSC. It gives a coupling reactance between the converter and the AC system. The converter transformer can be used to reduce the fault current and size of the filter. The reactance value of the converter transformer is in the range of 0.1 to 0.2 p.u.

2.3 Phase Reactor

The phase reactor can be used to control the power flow of VSC by altering the current flow through it. Also, it can be used as the filter to mitigate the high-frequency harmonic contents of AC currents. The phase reactor value is taken as 0.15 per unit for the design calculation. It can be designed using the following relations [13].

The base current and impedance are given by,

$$I_B = \frac{S_B}{\sqrt{3}\times V_B} \quad ; \quad Z_B = \frac{V_B/\sqrt{3}}{I_B} \tag{9}$$

phase A reactance,

$$X_{LA} = 0.15 \text{ p.u.} \times Z_B \tag{10}$$

phase A inductance,

$$L_A = \frac{X_{LA}}{\omega} \tag{11}$$

Nominal reactive power of phase A reactance is given by,

$$Q_{XLA} = I_A^2 \times X_{LA} \tag{12}$$

where I_A is the phase A current.

2.4 AC Filters

In the HVDC system, the harmonic voltages and currents can be generated due to the non-uniform distribution of flux on the armature winding of the AC generator, saturation of the converter transformer and switching of the PWM converter. The switching instant of VSC and the resonance between L and C are the main reason for the generation of high-frequency harmonics. In particular, switching frequency is the primary source of harmonics. The harmonic voltage will be very high magnitude when the harmonic frequency is equal to the switching frequency. The high pass filter (HPF) can be applied to mitigate the high-frequency harmonics, and its design can be done using the following relations [14].

$$C_f = \frac{Q_f}{2 \times \pi \times f \times V_L^2} \tag{13}$$

$$R_f = \frac{1}{2 \times \pi \times f_{cut-off} \times C_f} \tag{14}$$

$$L_f = m \times R_f^2 \times C_f \tag{15}$$

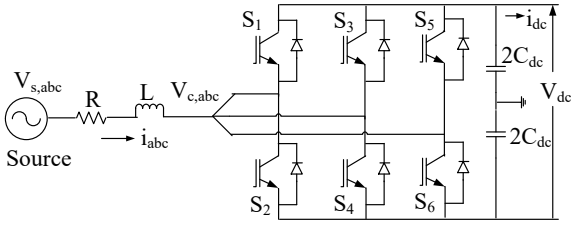

Fig.4: *AC source connected VSC.*

where Q_f is the reactive power rating of HPF, $f_{cut-off}$ is the cut-off frequency, V_L is the line-to-line voltage, f is the fundamental frequency, m is the parameter which relates the shape of filter impedance and the frequency curve. It can be varied from 0.5 to 2.

2.5 Control Model for VSC-HVDC

The VSCs are developed based on insulated gate bipolar transistor (IGBT) switches with turn-on and turn-off capabilities. It uses six switch valves which contain many switches in series depending on the voltage and current ratings. The two-level topologies are commonly used for the HVDC converters. The AC source connected HVDC converter, i.e., two-level VSC is shown in Fig. 4.

The three-phase AC voltage at source terminal ($V_{s,\ abc}$) is given by,

$$V_{s,abc} = Ri_{abc} + L\frac{di_{abc}}{dt} + V_{c,abc} \tag{16}$$

where $V_{c,abc}$ is the three-phase AC voltage at converter terminal, i_{abc} is the AC current, R and L are the resistance and inductance respectively. Consider the q-axis of the rotor reference frame is aligned to the AC voltage vector, and the q-axis is leading the d axis by 90°. Convert the Eq. (16) from abc to $d-q$ form, the source voltage in the $d-q$ frame is given by,

$$V_{s,q} = Ri_q + L\frac{di_q}{dt} + \omega L i_d + V_{c,q} \tag{17}$$

$$V_{s,d} = Ri_d + L\frac{di_d}{dt} - \omega L i_q + V_{c,d} \tag{18}$$

where $V_{c,d}$ and $V_{c,q}$ are the converter voltage in the $d-q$ frame, i_d and i_q represent the d and q components of current and ω is the supply frequency. The following relations can be used to control the active power (P) and DC voltage (V_{dc}) as given by,

$$P = \frac{3}{2}\left(V_{s,d}i_d + V_{s,q}i_q\right) \tag{19}$$

$$P_{dc} = V_{dc}i_{dc} \tag{20}$$

where i_{dc} is the DC current.

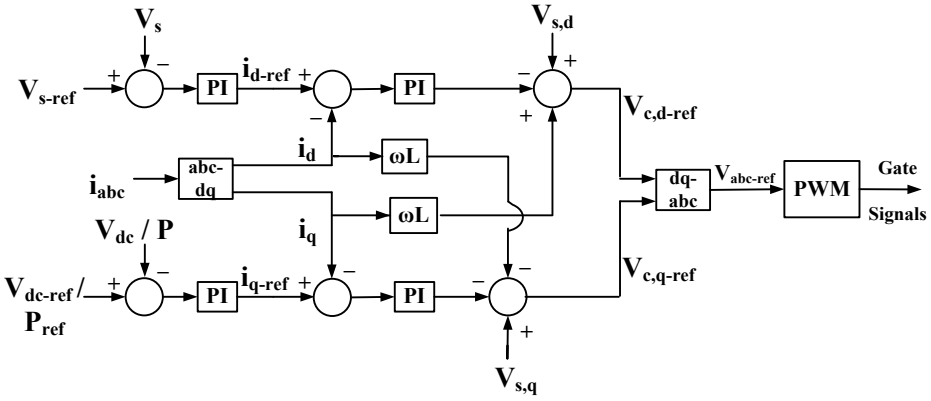

Fig.5: *Control block diagram for VSC-HVDC.*

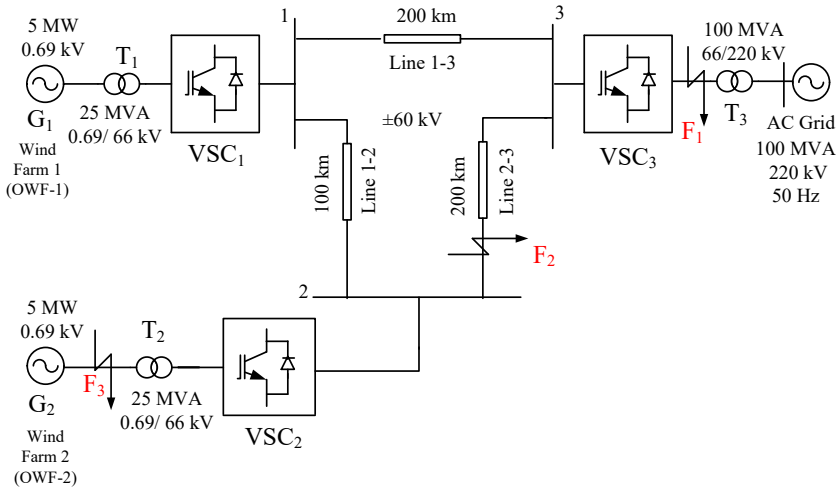

Fig.6: *Test Case 1 - Three-terminal HVDC transmission system.*

Vector control is used as the control system for VSC which is shown in Fig. 5. It can be developed based on the Eqs. (17)–(20). It contains an inner current and outer controller. The DC voltage (V_{dc}) and AC voltage (V_s) controller is modeled as an outer controller for the OWF side converter, and it regulates the V_{dc} and V_s under variable conditions. The active power (P) and AC voltage (V_s) controller is modeled as an outer controller for the grid side converter, and it regulates the voltage of HVDC grid and maintains the PCC voltage by providing the reactive power support. The current controller is independently controlling the $d-q$ axis components of the current. The generated $d-q$ axis components of reference voltages are transformed back to the three-phase abc frame and given as a reference signal for the sinusoidal pulse width modulation (SPWM) which can be used to produce the switching pulses for the VSC [15–17].

2.6 DC Capacitor

DC capacitor is the energy storage component of VSC, and it can be used to maintain the DC voltage between the switching instants. The primary consideration while designing the C_{dc} is to limit the DC voltage ripple, reduce the harmonic content of the DC side and also to limit the peak discharging current under DC fault conditions. The DC capacitor (C_{dc}) can be calculated by,

$$C_{dc} = \frac{2S_{VSC}E_s}{V_{dc}^2} \tag{21}$$

$$E_s = \frac{E_c}{S_{VSC}} \quad ; \quad E_c = \frac{1}{2}C_{dc}V_{dc}^2 \tag{22}$$

where V_{dc} is the rated DC voltage, S_{VSC} is the converter power in VA, E_c is the capacitor energy in J and E_s is the energy to power ratio in J/VA. The E_s can be varied from 10 to 50 kJ/MVA [18].

2.7 DC Transmission Line

Frequency-dependent phase model is used for the multi-terminal HVDC line due to the accurate representation of the frequency dependency and distributed nature of all parameters. It can be called a distributed RLC traveling wave model and is also

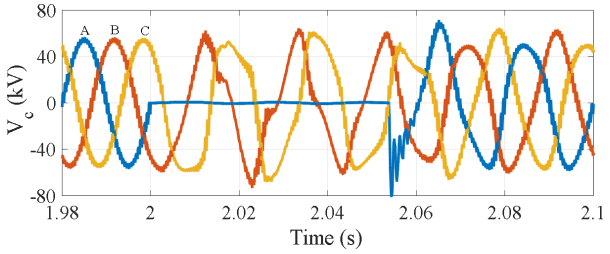

(a) Three-phase AC voltage (V_c) at LV side of T_3.

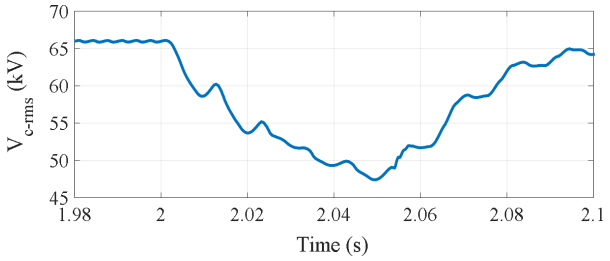

(b) Line-to-Line RMS voltage (V_{c-rms}) at LV side of T_3.

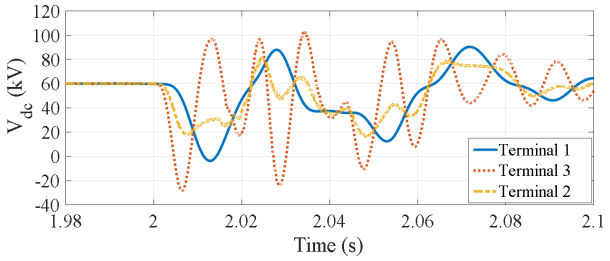

(c) Positive pole-to-ground DC voltage (V_{dc}) at the terminal-1,2,3 of the HVDC system.

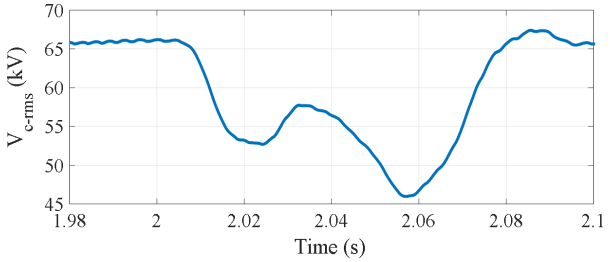

(d) Line-to-Line RMS voltage (V_{c-rms}) at HV side of transformer T_1 (OWF side).

Fig.7: *The response of the proposed HVDC System under A-G fault at LV side of* T_3.

widely used for PSCAD simulation studies. It can eliminate the problems associated with the modal transformation matrices due to the direct formulation of the phase domain. The detailed modeling of the DC line and its data is given in [19–22].

3. SIMULATION STUDIES

In this section, different case studies are carried out to evaluate the transient performance of the MT VSC-HVDC transmission system linked OWFs under power system disturbances such as fault conditions including wind variabilities using PSCAD/EMTDC simulation. The main purpose of this study is to understand the transient behavior of the MT VSC-HVDC transmission system linked OWFs.

3.1 Test Case 1

The three-terminal VSC-HVDC transmission system linked OWFs is shown in Fig. 6. The offshore wind power generation of each unit has 5 MW, 0.69 kV capacity. The offshore wind power is stepped-up to the transmission level as 66 kV using a converter transformer. The OWF VSCs, i.e., VSC_1 and VSC_2 are connected by 100 km distance, and these are connected to VSC_3 by 200 km distance. The mesh connection is used for the three-terminal HVDC network due to the advantage of high flexibility and reliability. Symmetric monopolar configuration is applied for the HVDC link operation, and it provides three voltage levels $\left(\frac{+V_{DC}}{2},\ 0,\ \frac{-V_{DC}}{2}\right)$, where V_{DC} is the pole-to-pole DC voltage. The pole-to-ground DC voltage (V_{dc}) is ±60 kV in steady state condition. The output of VSC_3 is stepped-up to grid voltage level as 220 kV, and finally, it has connected to the AC grid [23].

3.1.1 System Response under Phase-to-Ground Fault on Grid Side

The phase-to-ground (A-G) fault is applied on LV side of the converter transformer T_3 which is indicated as F_1 in Fig. 6. The A-G fault is created at time t = 2.0 s, the fault duration is considered as 0.05 s, and the fault resistance (R_f) is taken as 0.05 Ω. The response of the HVDC system under A-G fault is shown in Fig. 7.

After the occurrence of a fault, the AC voltage at LV side of T_3 has decreased from 66 kV to 48 kV and recovers slowly to the nominal value after clearance of the fault which can be seen from the Fig. 7(a) and (b). Fig. 7(c) indicates that the transients are produced in the DC voltage at the terminal-1,2,3 of HVDC system due to the fault on AC side. The AC voltage at the HV side of T_1, i.e., the response of the OWF side also gets affected due to the A-G fault on grid side as shown in Fig. 7(d).

3.2 System Response under DC Pole-to-Pole Fault on Line 2-3

The DC pole-to-pole fault is applied at terminal-2 in the three-terminal HVDC system which is indicated as F_2 in Fig. 6. The DC fault is created at time t = 2.0 s, the fault duration is considered as 0.05 s, and the short circuit fault resistance is taken as 0.01 Ω. The response of the HVDC system under DC pole-to-pole fault is shown in Fig. 8.

After the occurrence of a fault, the DC link capacitor starts to discharge, i.e., the DC voltage at the terminal-1,2,3 of the HVDC system are reduced to zero within a few milliseconds as shown in Fig. 8(a). The DC fault current will flow in the diode path of the VSC since the IGBTs are blocked by self-protection. The peak value of DC fault current at terminal-2

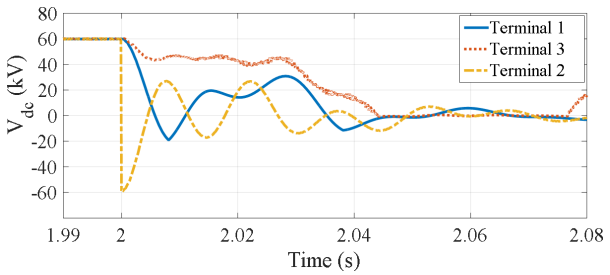

(a) Positive pole-to-ground DC voltage (V_{dc}) at the terminal-1,2,3 of the HVDC system.

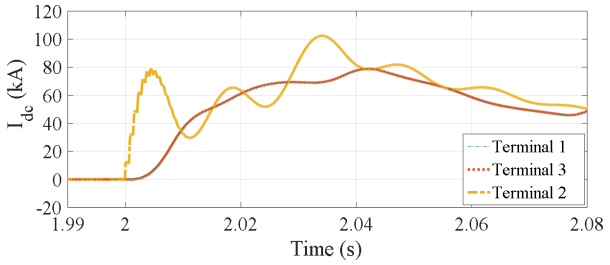

(b) DC current (I_{dc}) at the terminal-1,2,3 of the HVDC system.

Fig.8: *The response of the proposed HVDC system under DC pole-to-pole fault at terminal-2.*

has raised up to 102 kA within a few ms, and the peak fault current at terminal-1 and terminal-3 are increased up to 79 kA which can be seen from the Fig. 8(b). The major portion of transients which is generated by the DC fault has come from discharging of energy storage elements such as DC capacitor and line inductor.

From the simulation results of AC and DC faults, it can be seen that the DC fault current has low rise time and high steady-state values during the transient phases. Therefore, the performance of MT VSC-HVDC system has been severely affected due to the fault on the DC side.

3.2.1 System Response under Gust Wind with Phase-to-ground Fault on OWF-2

The performance of the proposed HVDC system is analyzed under gust wind during phase-to-ground fault (A-G) condition. Gust wind is applied at time $t = 1.0$ s. Gust peak velocity is considered as 12 m/s, gust period is taken as 3 s, gust starting time is set as 1 s, the number of the gust is considered as 1. The normal wind speed is 12 m/s. Therefore, the peak value of wind speed can go up to 24 m/s. The A-G fault is applied at the PMSG terminal of OWF-2 (G_2) which is indicated as F_3 in Fig. 6. The fault is created at $t = 1.5$ s, the fault duration is considered as 0.05 s, and the R_f is taken as 0.04 Ω. Fig. 9 shows the response of the HVDC system under gust wind during A-G fault at PMSG terminal of OWF-2.

Fig. 9(a) indicates the variation of wind speed in the form of a gust pattern in the OWF-2. The AC voltage and active power at PMSG terminal give an oscillation due to the gust wind as shown in Fig. 9(b) and (c). During the A-G fault with gust wind, the variation of AC voltage at PMSG and converter terminal is higher when compared to the case of steady-

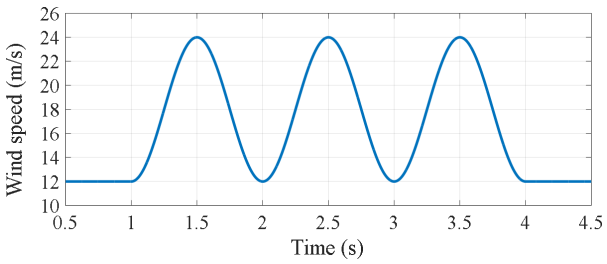

(a) Gust wind speed.

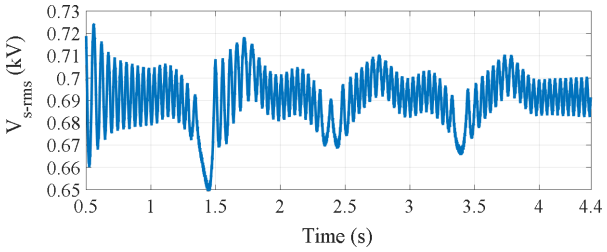

(b) RMS voltage (V_{s-rms}) at PMSG terminal of OWF-2.

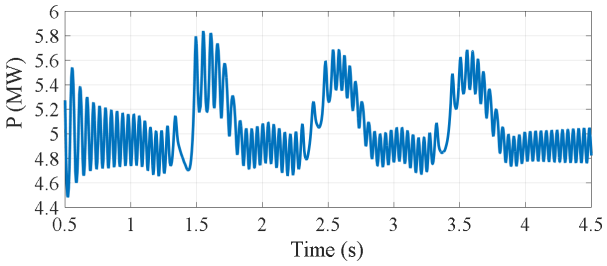

(c) Active power (P) at PMSG terminal of OWF-2.

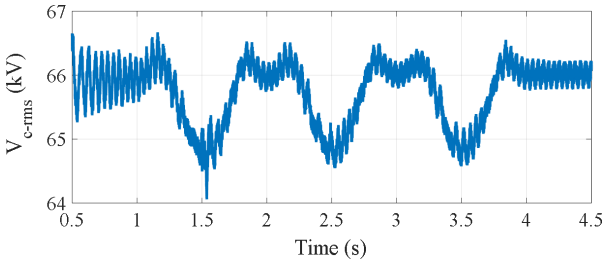

(d) RMS Voltage (V_{c-rms}) at HV side of T_2.

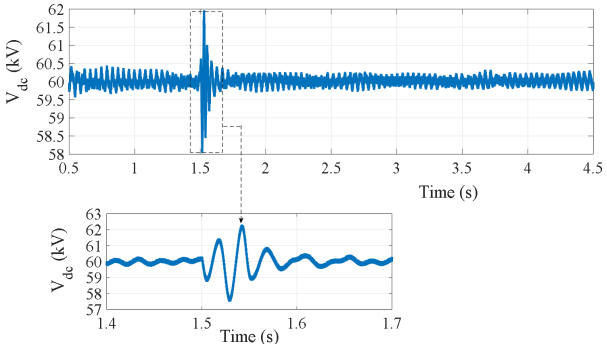

(e) Positive pole-to-ground DC Voltage (V_{dc}) at VSC_2.

Fig.9: *The response of the proposed HVDC system under gust wind during A-G fault at PMSG terminal of OWF-2.*

state with gust wind which can be observed from Fig. 9(b) and (d). The transients are present in the DC voltage during the fault period as shown in Fig. 9(e). However, the gust wind has no influence on the DC voltage due to the $d-q$ controller of VSC and the configuration of the MT HVDC network.

3.2.2 System Response under Ramp Wind with Phase-to-Ground Fault on OWF-2

The performance of the proposed HVDC system is analyzed under ramp wind during A-G fault condition. The normal wind speed is set to 12 m/s. The ramp wind is created at time $t = 1.0$ s. Ramp maximum velocity is considered as 12 m/s, ramp period is taken as 1 s, and ramp starting time is set as 1 s, the number of ramps is considered as 3. The A-G fault is applied at PMSG terminal of OWF-2 (G_2) which is indicated as F_3 in Fig. 6. The A-G fault is applied at time $t = 3$ s, the fault duration is considered as 0.05 s, and the R_f is taken as 0.04 Ω. Fig. 10 shows the response of HVDC system under ramp wind during A-G fault at PMSG terminal of OWF-2.

Fig. 10(a) indicates the variation of wind speed in the form of a ramp pattern in the OWF-2. At time $t = 3.0$ s, the variation of AC voltage and active power at PMSG terminal is more significant when compared to time $t = 2.0$ s and $t = 4.0$ s which can be seen from the Fig. 10(b) and (c). The AC voltage at the HV side of T_2 has decreased to 64.5 kV as shown in Fig. 10(d). The transients are present in the DC voltage due to A-G fault as shown in Fig. 10(e). Therefore, the performance of the HVDC system gets affected during A-G fault under ramp wind condition.

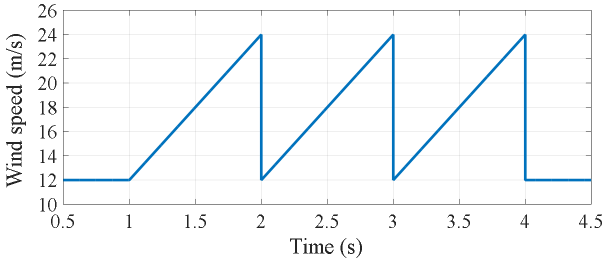

(a) Ramp wind speed.

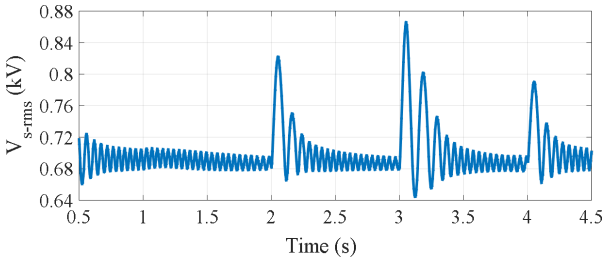

(b) RMS voltage (V_{s-rms}) at PMSG terminal of OWF-2.

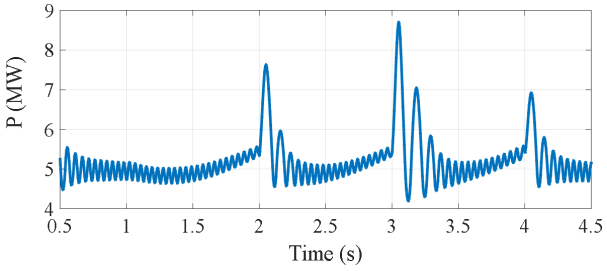

(c) Active power (P) at PMSG terminal of OWF-2.

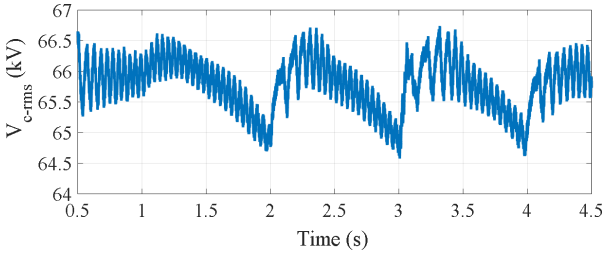

(d) RMS Voltage (V_{c-rms}) at HV side of T_2.

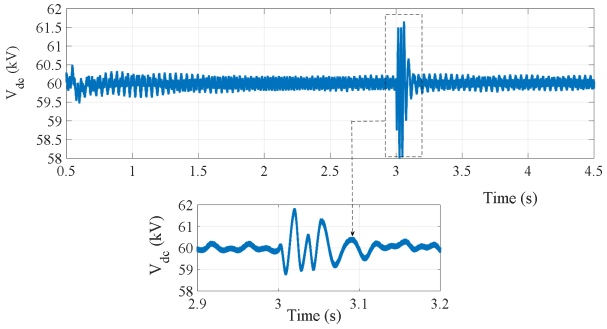

(e) Positive pole-to-ground DC Voltage (V_{dc}) at VSC_2.

Fig.10: *The response of the proposed HVDC system under ramp wind during A-G fault at PMSG terminal of OWF-2.*

3.3 Test Case 2

The second test case of the three-terminal HVDC system for the connection of OWFs with the AC grid is shown in Fig. 11. The output of each OWF unit is 5 MW, 0.69 kV capacity. The generated offshore wind power is boosted to the medium voltage level of 33 kV by using 5 MVA, 0.69/33 kV transformer. The rating of the AC source is 5 MVA, 33 kV. The wind farm unit and AC source are connected to the 33 kV bus. The medium voltage is boosted to the transmission level of 66 kV by using 25 MVA, 33/66 kV transformer. The vector controlled VSC is used to connect the three-terminal HVDC with the AC grid. The pole-to-ground DC voltage is ±150 kV in steady state condition. The output of the grid-connected VSC (VSC_3) is 132 kV, and it is boosted to a grid voltage level as 220 kV by using 100 MVA, 132/220 kV transformer.

3.3.1 System Response under Three Phase-to-ground Fault on VSC_2

The three phase-to-ground fault is applied at the HV side of T_4 which is given as F_1 in Fig. 11. The fault is created at time $t = 2.0$ s, the fault duration is considered as 0.05 s, and the R_f is taken as 0.02 Ω. The response of the HVDC system under three phase-to-ground fault is shown in Fig. 12.

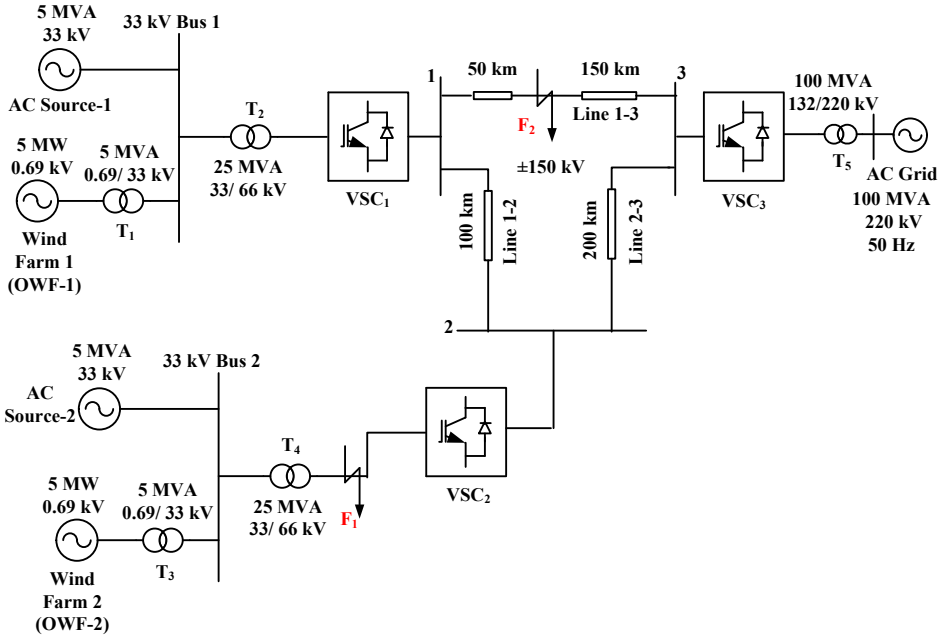

Fig.11: *Test Case 2 - Three-terminal HVDC transmission system.*

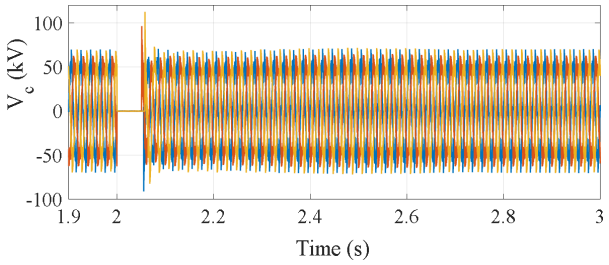

(a) Three-phase AC voltage (V_c) at HV side of T_4.

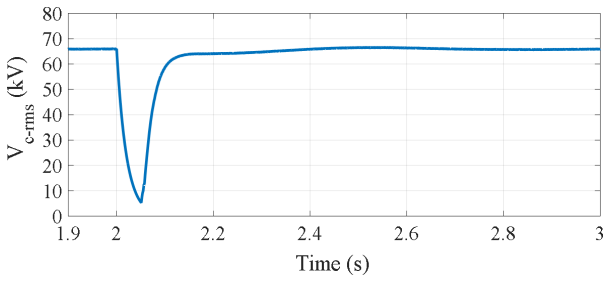

(b) RMS voltage (V_{c-rms}) at HV side of T_4.

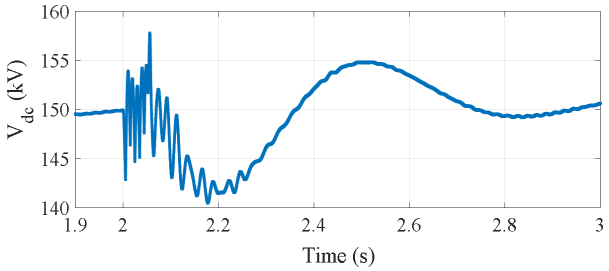

(c) Positive pole-to-ground DC voltage (V_{dc}) at VSC_2.

Fig.12: *The response of the proposed HVDC system under ramp wind during A-G fault at PMSG terminal of OWF-2.*

The AC voltage at the converter terminal has decreased nearer to zero during fault period, and it starts increasing after the clearance of fault as shown in Fig. 12(a) and (b). The response of the DC system is that the DC voltage gets disturbed due to the three phase-to-ground fault at the HV side of T_4 which can be seen from the Fig. 12(c).

3.3.2 System Response under DC Pole-to-Pole Fault on Line 1-3

The DC pole-to-pole fault is applied at 50 km distance from terminal-1 and 150 km distance from terminal-3 which is indicated as F_2 in Fig. 11. The DC pole-to-pole fault is created at $t = 2.0$ s, the fault duration is considered as 0.05 s, and the short circuit fault resistance is taken as 0.01 Ω. The response of the proposed HVDC system under DC pole-to-pole fault is shown in Fig. 13.

After the occurrence of the DC pole-to-pole fault, the DC voltage measured at the terminal-1,2,3 of the HVDC system is decreased to zero within a few ms which can be seen from Fig. 13(a). The DC fault current measured at terminal-1 has raised to 59.32 kA within a short period, and the peak fault current at terminal-3 and terminal-2 are 34.6 kA and 4.67 kA which is given in Fig. 13(b). Therefore, the response of the HVDC system is significantly affected due to DC pole-to-pole fault cases. From the results, it can be noticed that the DC faults are having higher peak and steady fault currents which can damage the power electronic converters, circuit breakers, and other AC system components.

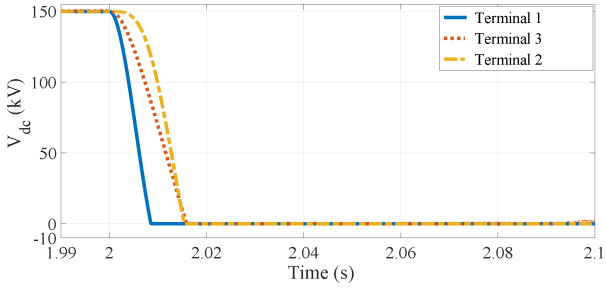

(a) Positive pole-to-ground DC voltage (V_{dc}) at the terminal-1,2,3 of the HVDC system.

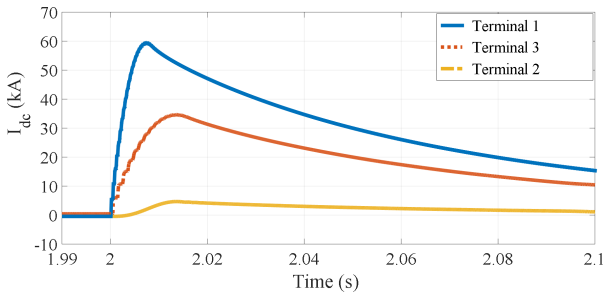

(b) DC current (I_{dc}) at the terminal-1,2,3 of the HVDC system.

Fig.13: *The response of the proposed HVDC system under DC pole-to-pole fault at 50 km distance from terminal-1.*

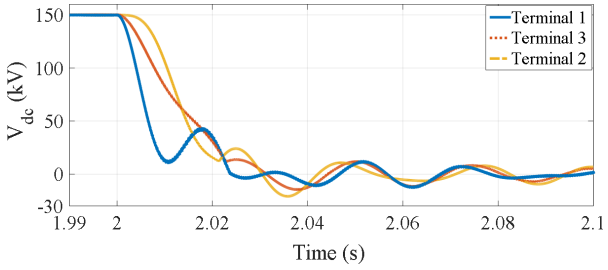

(a) Positive pole-to-ground DC voltage (V_{dc}) at the terminal-1,2,3 of the HVDC system.

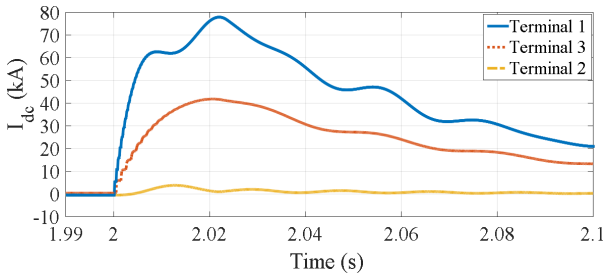

(b) DC current (I_{dc}) at the terminal-1,2,3 of the HVDC system.

Fig.14: *The response of the proposed HVDC system under DC positive pole-to-ground fault at 50 km distance from terminal-1.*

3.3.3 System Response under DC Pole-to-Ground Fault on Line 1-3

The DC positive pole-to-ground fault is applied at 50 km distance from terminal-1 and 150 km distance from terminal-3 which is indicated as F_2 in Fig. 11. The fault is created at $t = 2.0$ s, the fault duration is considered as 0.05 s, and the R_f is taken as 0.04 Ω. The response of the HVDC system under DC positive pole-to-ground fault is shown in Fig. 14.

The pole-to-ground fault dependis on the grounding of the HVDC system. After the occurrence of a fault, the DC voltage measured at the terminal-1,2,3 of the HVDC system are reduced abnormally as shown in Fig. 14(a). The peak value of DC fault current at terminal-1 has increased to 78 kA within a few ms. The peak value of DC fault current at the terminal-3 and terminal-2 has increased up to 42 kA and 4 kA which can be observed from the Fig. 14(b). In the pole-to-ground fault case also, the DC fault current has reached an abnormal value which is not an acceptable limit of rating of components used in the HVDC system.

4. CONCLUSIONS

In this paper, the design and modeling of MT VSC-HVDC transmission system linked OWFs are presented. Simulation studies are carried out to analyze the transient performance of the three-terminal VSC-HVDC transmission system under fault conditions. The obtained results indicate that the DC fault has the higher peak and steady fault currents with low-rise time and more attention is required for DC faults in the multi-terminal VSC-HVDC link operation. In addition, simulation studies are carried out to test the transient performance of three-terminal HVDC transmission system under the variation of wind speed as in the form of gust and ramp pattern during both steady state and fault conditions. From the obtained results it is observed that the variation of wind speed has a significant impact on the response of the PMSG output terminal and HV side of the converter transformer, and no effect on the response of the DC side of HVDC system.

5. APPENDIX

The model calculation for the design of test case 1–three-terminal HVDC transmission system linked OWFs which consists of wind source and grid connected VSC is presented in the following sections.

5.1 Wind Farm Connected VSC

The wind source connected to the HVDC converter (VSC_1) is given in Fig. 15. The rating of wind-turbine generator output = 5 MW, 0.69 kV, 50 Hz; converter transformer (T_1) = 25 MVA, 0.69/66 kV, leakage reactance = 10%. Phase reactor calculation for 25 MVA, 66 kV rating is given as: phase reactor = 0.15 p.u., the base current

$$I_B = \frac{S_B}{\sqrt{3}\times V_B} = \frac{25}{\sqrt{3}\times 66} = 0.2186 \text{ kA}$$

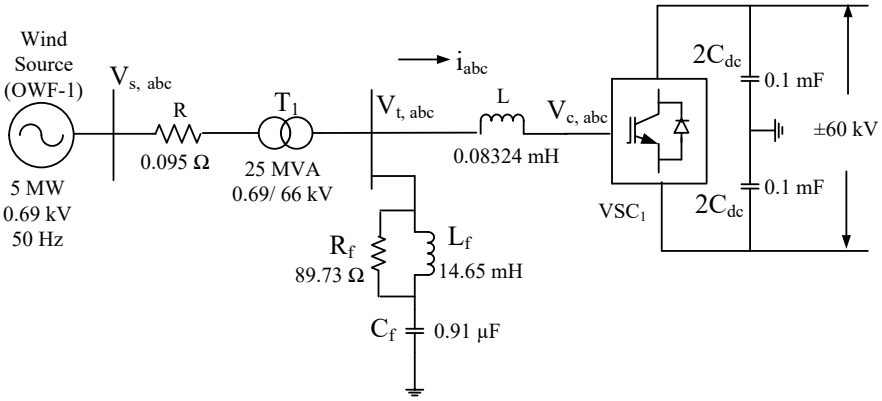

Fig.15: *OWF-1 connected VSC_1.*

the base impedance,

$$Z_B = \frac{66/\sqrt{3}}{0.2186} = 174.31\ \Omega$$

phase A reactance,

$$X_{LA} = 0.15\ \text{p.u.} \times 174.31 = 26.146\ \Omega$$

phase A inductance,

$$L_A = \frac{X_{LA}}{\omega} = 0.08324\ \text{H}$$

The nominal reactive power of phase A reactance is given by,

$$Q_{XLA} = I_A^2 \times X_{LA} = 1.2494\ \text{Mvar}$$

The design of high pass filter for 1.2494 Mvar and 1950 Hz cut-off frequency is given below:

$$C_f = \frac{Q_f}{2 \times \pi \times f \times V_L^2} = 0.91\ \mu\text{F}$$
$$R_f = \frac{1}{2 \times \pi \times f_{cut-off} \times C_f} = 89.73\ \Omega$$
$$L_f = m \times R_f^2 \times C_f = 14.65\ \text{mH}$$

In the Vector Controlled VSC, the AC voltage vector is aligned to the q-axis of the rotor reference frame. The q-axis is leading the d-axis by 90°. The calculation used for the decoupled $d-q$ controller is given by,

$$V_q^{base} = \sqrt{\frac{2}{3}} \times V_{ac}^{base} = 0.8164 \times 66\ \text{kV} = 53.88$$
$$i_{ac}^{base} = \frac{S_B}{\sqrt{3} \times V_{ac}^{base}} = \frac{25\ \text{MVA}}{\sqrt{3} \times 66\ \text{kV}} = 0.2186\ \text{kA}$$
$$i_q^{base} = \sqrt{2} \times i_{ac}^{base} = \sqrt{2} \times 0.2186 = 0.3091$$

modulation index $M = 0.898$, switching frequency = 1950 Hz. The output voltage of PWM-based three-phase VSC is given by,

$$V_{LL-rms} = \frac{\sqrt{3}}{2\sqrt{2}} \times M \times V_{DC} = 0.612 \times M \times V_{DC}$$

pole-to-pole DC voltage,

$$V_{DC} = \frac{66\ \text{kV}}{0.612 \times 0.898} = 120\ \text{kV}$$

pole-to-ground, DC voltage $V_{dc} = \pm 60$ kV (symmetric monopole configuration); DC capacitor,

$$C_{dc} = \frac{2S_{VSC}E_s}{V_{dc}^2} = 0.05\ \text{mF}$$

$2C_{dc} = 0.1$ mF; DC transmission line data is given by, $R = 0.0114\ \Omega$/km; $L = 0.8273$ mH/km; and $C = 0.0139\ \mu$F/km.

5.2 Grid Connected VSC

The AC source connected to the HVDC converter (VSC_3) is given in Fig. 16, AC Source = 100 MVA, 220 kV, 50 Hz; converter transformer = 100 MVA, 220/66 kV, leakage reactance = 10%. Phase reactor calculation for 100 MVA, 66 kV rating is given below: the base current,

$$I_B = \frac{S_B}{\sqrt{3}V_B} = \frac{100}{\sqrt{3} \times 66} = 0.8747\ \text{kA}$$

the base impedance,

$$Z_B = \frac{66/\sqrt{3}}{0.8747} = 43.56\ \Omega$$

phase A reactance,

$$X_{LA} = 0.15\ \text{p.u.} \times 43.56 = 6.5345\ \Omega$$

phase A inductance

$$L_A = \frac{X_{LA}}{\omega} = 0.0208\ \text{H}$$

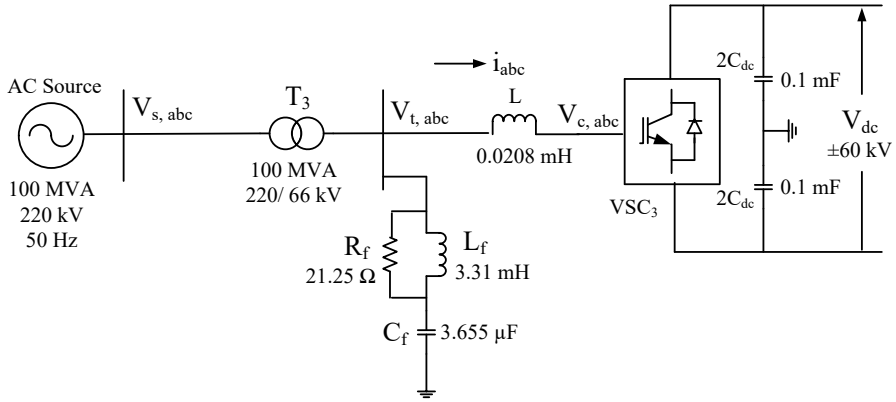

Fig.16: *Grid connected VSC_3.*

Nominal reactive power of phase A reactance is given by,

$$Q_{XLA} = I_A^2 \times X_{LA} = 5 \text{ Mvar}$$

High pass filter for 5 Mvar and 2050 Hz cut-off frequency is given below:

$$C_f = 3.655 \ \mu\text{F} \ ; \ R_f = 21.25 \ \Omega \ ; \ L_f = 3.31 \text{ mH}$$

Here also, the stator voltage is aligned to q-axis. The q-axis is leading the d-axis by 90°. The calculation used for the decoupled $d-q$ controller is given by,

$$i_{ac}^{base} = 0.8747 \text{ kA}$$
$$V_q^{base} = 53.88$$
$$i_q^{base} = 1.237$$

pole-to-pole DC voltage, $V_{DC} = 120$ kV; pole-to-ground DC voltage, $V_{dc} = \pm 60$ kV; DC capacitor, $C_{dc} = 0.05$ mF, $2C_{dc} = 0.1$ mF.

Then, the wind source connected VSC can be linked with the grid-connected VSC using the meshed multi-terminal HVDC transmission system.

References

[1] R. Perveen, N. Kishor, and S. R. Mohanty, "Offshore wind farm development: Present status and challenges," *Renew. Sustain. Energy Rev.*, vol. 29, pp. 780-792, Jan. 2014.

[2] M. R. Islam, Y. Guo, and J. Zhu, "A review of offshore wind turbine nacelle: Technical challenges, and research and development trends," *Renew. Sustain. Energy Rev.*, vol. 33, pp. 161-176, May 2014.

[3] C. M. Franck, "HVDC circuit breakers: a review identifying future research needs," *IEEE Trans. Power Del.*, vol. 26, no. 2, pp. 998-1007, Apr. 2011.

[4] L. Xu, L. Yao, and C. Sasse, "Grid integration of large DFIG-based wind farms using VSC transmission," *IEEE Trans. power sys.*, vol. 22, no. 3, pp. 976-984, Aug. 2007.

[5] K. Mohamed, Z. Ahmed, H. Samir, F. Karim, and A. Rabie, "Performance analysis of a voltage source converter (VSC) based HVDC transmission system under faulted conditions," *Leonardo Journal of Sciences*, vol. 8, no. 15, pp. 33-46, July, 2009.

[6] R. E. Torres-Olguin, M. Molinas, and T. Undeland, "Offshore wind farm grid integration by VSC technology with LCC based HVDC transmission," *IEEE Trans. Sustain. Energy*, vol. 3, no. 4, pp. 899-907, Oct. 2012.

[7] J. P. Rodriguez, "Dynamic averaged models of VSC-based HVDC systems for electromagnetic transient programs," Ph.D. Dissertation, Univ. of Montreal, Canada, 2013.

[8] F. Deng, and Z. Chen, "An offshore wind farm with DC grid connection and its performance under power system transients," in *Proc. IEEE Power Energy Soc. Gen. Meeting*, pp.1-7, 2011.

[9] J. G. Slootweg, S. W. H. De Haan, H. Polinder, and W. L. Kling, "General model for representing variable speed wind turbines in power system dynamics simulations," *IEEE Trans. power sys.*, vol. 18, no. 1, pp. 144-151, Feb. 2003.

[10] O. Carranza, E. Figueres, G. Garcerá, and R. Gonzalez-Medina, "Analysis of the control structure of wind energy generation systems based on a permanent magnet synchronous generator," *Appl. Energy*, vol. 103, pp. 522-538, Mar. 2013.

[11] P. Krause, O. Wasynczuk, S. D. Sudhoff, and S. Pekarek, *Analysis of electrical machinery and drive systems,* Wiley, Hoboken, NJ, USA, 2013.

[12] D. Y. Ohm, *Dynamic Model of PM Synchronous Motors,* Drivetech, Inc., Blacksburg, Virginia, 2000.

[13] D.P. Dorantes, J. L. M. Morales, and M. H. Ángeles, "A filter design methodology of a VSC-HVDC system," in *2013 IEEE International Autumn Meeting on Power Electronics and Computing (ROPEC)*, pp. 1-6, 2013.

[14] G. Shi, X. Cai, and Z. Chen, "Design and control of multi-terminal VSC-HVDC for large offshore

wind farms," *Przeglad Elektrotechniczny*, vol. 88, no. 12a, pp. 264- 268, 2012.

[15] E. Kontos, R. T. Pinto, and P. Bauer, "Control and protection of VSC-based multi-terminal DC networks," Masters Thesis, Delft Univ. of Technology, Delft, Netherlands, 2013.

[16] C. Bajracharya, M. Molinas, J. A. Suul, and T. M. Undeland, "Understanding of tuning techniques of converter controllers for VSC-HVDC," in *Proc. Nordic Workshop on Power and Ind. Electron. (NORPIE/2008)*, pp. 1-6, 2008.

[17] L. Xu, and S. Li, "Analysis of HVDC control using conventional decoupled vector control technology," in *Proc. IEEE Power Energy Soc. Gen. Meeting*, pp. 1-8, 2010.

[18] D. Jovcic, and K. Ahmed, *High voltage direct current transmission: converters, systems and DC grids*, Wiley, Scotland, UK, 2015.

[19] *PSCAD/EMTDC online help system,* version 4.6, Manitoba HVDC Research Centre, Canada.

[20] J. R. Marti, "Accurate modeling of frequency-dependent transmission lines in electromagnetic transient simulations," *IEEE Trans. Power App. Syst.*, vol. PAS-101, no. 1, p. 147, 1982.

[21] J. R. Marti, L. Marti, and H. W. Dommel, "Transmission line models for steady-state and transients analysis," in *Proc. IEEE/Nat. Tech. Univ. Athens Power Tech. Conf.: Planning, Operation, Control of Todayś Electric Power Systems*, pp. 744-750, 1993.

[22] K. Vrana, S. Dennetière, J. Jardini, Y. Yang, D. Jovcic, and H. Saad, "The CIGRE B4 DC grid test system," in *Electra*, pp. 10-19, 2013.

[23] M. Mohan, and K. Panduranga Vittal, "Modeling and simulation studies on performance evaluation of three-terminal VSC-HVDC link connected offshore wind farms," in *Proc. IEEE International Conference on Energy, Communication, Data Analytics and Soft Computing (ICECDS)*, pp. 473-478, 2017.

M. Mohan received his B.E. (Electrical and Electronics) degree from Christian College of Engineering and Technology, Dindigul, India in 2010 and M.E. (Power Systems) degree from Thiagarajar College of Engineering, Madurai, India in 2012. He has completed his Ph.D. degree from National Institute of Technology Karnataka (NITK), Surathkal, India in 2019. Presently he is serving as an Assistant Professor in the Department of Electrical and Electronics Engineering, CMR Institute of Technology, Bengaluru. His research interests include HVDC and FACTS, Power system protection, AC/DC Microgrid, and Grid integration of large-scale wind farms.

K. Panduranga Vittal received his B.E. (Electrical and Electronics) degree from Mysore University, India in 1985, M.E. (Applied Electronics) degree from PSG College of Technology, Coimbatore, India in 1989, and Ph.D. degree from National Institute of Technology Karnataka (NITK), Surathkal, India in 1999. Presently he is serving as Professor in the Department of Electrical & Electronics Engineering, NITK Surathkal, India. He has published around 25 technical research papers in International Journals and 70 papers in various National and International conferences. His research interests include power system protection, transient behavioural modeling of power apparatus and FACTS devices.